



Halide perovskites enable polaritonic XY spin Hamiltonian at room temperature

Renjie Tao^{1,7}, Kai Peng^{2,7}, Louis Haeberlé^{1D}³, Quanwei Li^{1D}⁴, Dafei Jin^{1D}⁵, Graham R. Fleming⁴, Stéphane Kéna-Cohen^{1D}³, Xiang Zhang^{1D}⁶✉ and Wei Bao^{1D}²✉

Exciton polaritons, the part-light and part-matter quasiparticles in semiconductor optical cavities, are promising for exploring Bose-Einstein condensation, non-equilibrium many-body physics and analogue simulation at elevated temperatures. However, a room-temperature polaritonic platform on par with the GaAs quantum wells grown by molecular beam epitaxy at low temperatures remains elusive. The operation of such a platform calls for long-lifetime, strongly interacting excitons in a stringent material system with large yet nanoscale-thin geometry and homogeneous properties. Here, we address this challenge by adopting a method based on the solution synthesis of excitonic halide perovskites grown under nanoconfinement. Such nanoconfinement growth facilitates the synthesis of smooth and homogeneous single-crystalline large crystals enabling the demonstration of XY Hamiltonian lattices with sizes up to 10×10 . With this demonstration, we further establish perovskites as a promising platform for room temperature polaritonic physics and pave the way for the realization of robust mode-disorder-free polaritonic devices at room temperature.

Bose-Einstein condensation (BEC), first proposed in 1924, describes a quantum-statistical phase transition where, below the transition temperature, a substantial fraction of diluted bosonic particles spontaneously occupy the ground state and exhibit macroscopic quantum behaviours. The experimental realization of BEC condensates and their optical lattices in ultracold (approximately microkelvin) atoms enabled the field of analogue simulation, where complex many-body physics problems such as the formation of frustrated spin, superconductivity and superfluidity, to be experimentally tackled in a controllable manner^{1–3}. Because of the complexity and extremely low temperature involved in using ultracold atoms, there have been great efforts recently towards building a room-temperature analogue simulator with solid-state BEC systems for practical applications^{4–6}.

In this context, semiconductor microcavities are an attractive platform. In a semiconductor optical cavity, exciton polaritons, hybrid light-matter quasiparticles, are formed when the coupling rate between excitons and photons is much faster than their respective dissipation rates. These bosonic polaritons have an ultra-small effective mass ($\sim 10^{-5}$ electron mass) inherited from the photon, as well as nonlinear interactions inherited from the exciton Coulombic interactions. Thus, polaritons can undergo BEC at much-elevated temperatures^{4,6}, ultimately limited by the exciton binding energy. Polariton condensation was first realized in quantum-well microcavities grown with molecular beam epitaxy (MBE)^{7,8}, where liquid helium temperatures (~ 4 K) must be maintained to prevent exciton autoionization. Although high exciton binding energy materials, such as organic molecules, show potential for room-temperature polaritonics^{9–12}, they unfortunately have severe limitations on sample size, homogeneity, polariton lifetime and/or nonlinear interaction strength. Therefore, the large and homogeneous MBE-grown GaAs quantum well remains the only exciton-polariton platform (though at low temperature) where interesting physics, such as soliton

formation^{13,14}, XY spin Hamiltonian¹⁵ and topological effects^{16,17}, have been experimentally explored. This is primarily attributed to two reasons: the maturity of high-quality MBE material growth and patterning, and the strongly interacting excitons of the GaAs quantum wells at liquid helium temperature.

Recently, semiconducting lead halide perovskites have emerged as contenders to GaAs for polaritonics but at room temperature due to their large exciton binding energy^{18–20}, high photoluminescence (PL) quantum yield²¹, tunable bandgap²² and high room-temperature nonlinear interaction strength²³. With chemical vapour deposition (CVD), single-crystalline inorganic halide perovskites have shown polariton condensation^{24,25}. However, due to the limitations of the current growth methods and the fragile nature of perovskites, only small single crystals can be integrated into the optical cavity (Supplementary Fig. 1). Critically, the small sizes prohibit the studies of the aforementioned large-scale phenomena due to the limited lattice size and the restricted propagation lengths²⁶.

In this work, we overcome these limitations by direct solution growth of various types of large-area halide perovskite single crystals inside optical nanocavities. Due to the uniform confined environment, our solution growth approach shows uniformity, comparable to the MBE-grown GaAs quantum well, enabling submillimetre-size large single crystals with superb excitonic quality. These crystals with strongly interacting Wannier-Mott excitons allowed us to successfully demonstrate a polaritonic XY spin Hamiltonian with all-inorganic perovskite CsPbBr_3 at room temperature. Further, we show that a lattice with a large number of coherently coupled condensates up to 10×10 can be achieved. This is an important step towards the ultimate goal of realizing a room-temperature polaritonic platform on par with MBE-grown GaAs at low temperatures. In addition, we show that the dispersion of the perovskite system has unique advantages for future studies on synthetic non-Abelian gauge fields and topological physics. Our work establishes a robust

¹Nanoscale Science and Engineering Center, University of California, Berkeley, CA, USA. ²Department of Electrical and Computer Engineering, University of Nebraska-Lincoln, Lincoln, NE, USA. ³Department of Engineering Physics, École Polytechnique de Montréal, Montréal, Quebec, Canada. ⁴Department of Chemistry, University of California, Berkeley, CA, USA. ⁵Center for Nanoscale Materials, Argonne National Laboratory, Lemont, IL, USA. ⁶Faculty of Science and Faculty of Engineering, The University of Hong Kong, Hong Kong, China. ⁷These authors contributed equally: Renjie Tao, Kai Peng
✉e-mail: xiang@berkeley.edu; wbao@unl.edu

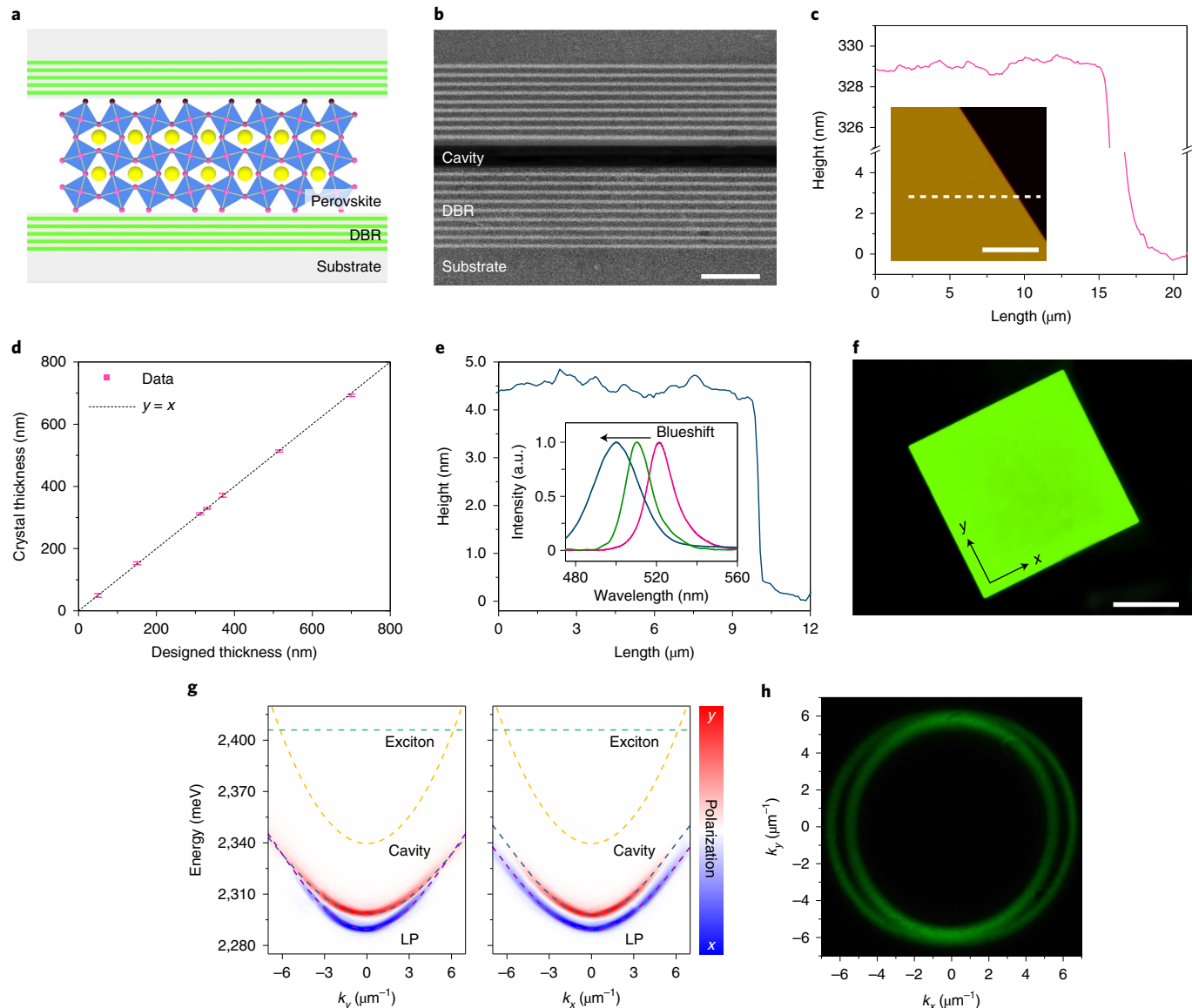


Fig. 1 | Synthesis and characterization of single-crystalline excitonic halide perovskites in DBR nanocavities. **a**, By using deposited pillar arrays (Supplementary Fig. 2) as spacers and bonders in between two DBR mirrors (nine pairs of SiO₂ and Ta₂O₅ alternating layers), a nanocavity of a designed height for halide perovskite crystals is formed so that the detuning between exciton and photon can be controlled. **b**, The scanning electron microscopy cross-sectional image of a fabricated nanocavity. Scale bar, 1 μm. **c**, The after-growth cavities are opened. The crystal thickness controllability and uniformity is revealed by AFM imaging (inset) and a cross-section profile (the white dashed line in the insert); the thickness of as-synthesized crystal from the nanocavity is ~329 nm (± 0.4 nm), which matches the designed height of the nanocavity (~330 nm). Scale bar, 10 μm. **d**, This nanometre-scale-precision thickness can be well controlled in a wide range as measured by AFM. The <1.6% of thickness variance across each chip (2 cm size) is caused by pillar film deposition uniformity. **e**, When shrinking the nanocavity height to only a few nanometres, the CsPbBr₃ crystals show a thickness of only 4.45 ± 0.35 nm and strong quantum-confinement-induced blueshifted PL (inset blue curve) down to 499 nm. The green curve in the inset corresponds to a measured thickness of 7.3 ± 0.5 nm (Supplementary Fig. 9b). **f**, A typical CsPbBr₃ crystal grown in the nanocavity shows uniform and bright PL across hundreds of micrometres. Scale bar, 100 μm. **g**, The linear-polarized PL of polariton dispersions (energy vs. wavevector k) along the y and x axes (two crystal axes as shown in **f**). The dashed lines are the fittings of the two lower branches (LP; red and blue), exciton energy (green) and cavity (orange) modes.. The two lower polariton branches with polarization along x (blue) and y (red) axis cross at the diabolic points at $k_y = 5.9 \mu\text{m}^{-1}$. **h**, The cross-section of the two polariton branches (PL measurement) in k -space at diabolic points with the energy of 2,332.5 meV, illustrating the Rashba-like spin-orbital coupling.

and excellent platform for room-temperature polaritonics and also paves the way for many other nonlinear polaritonic devices for practical applications.

Device synthesis and characterization

The key that enables our synthesis of high-quality perovskite crystals for large-scale polaritonics and the subsequent realization of

the polaritonic XY spin Hamiltonian at room temperature is the solution synthesis of halide perovskites directly within prefabricated optical nanocavities (a combination of top-down fabrication and bottom-up synthesis; schematic depiction in Supplementary Fig. 2), inspired by previous efforts in organic polariton growth²⁷ and recent halide perovskite growth²⁸. We first deposited high-quality distributed Bragg reflector (DBR) multilayers on the quartz

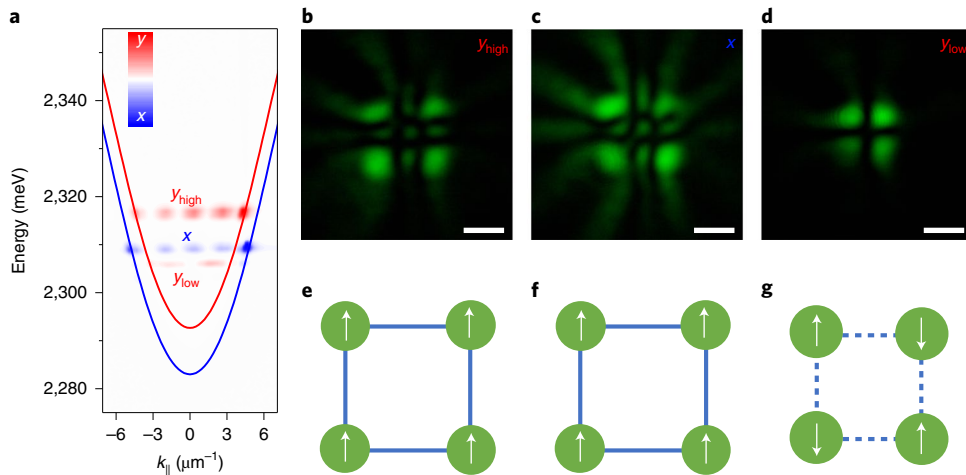


Fig. 2 | Room-temperature demonstration of polariton XY Hamiltonian square 2×2 lattices. **a-d**, Time-integrated k -space polariton dispersion before (the solid lines) and after (lines of dots) the condensation (**a**). The polariton condenses simultaneously at two lower branches with perpendicular polarization. At the branch with x polarization, the condensation occurs at $k_c = 4.95 \mu\text{m}^{-1}$. The odd number of interference fringes in the corresponding real-space image (**c**) shows an in-phase coupling. At the branch with y polarization, the condensation occurs at two different wave vectors (y_{high} , $k_c = 4.3 \mu\text{m}^{-1}$; y_{low} , $k_c = 3.2 \mu\text{m}^{-1}$). Panels **b** and **d** are the time-integrated real-space images of y_{high} and y_{low} , respectively. The intrinsic oscillatory lattice dynamics mechanism reduces the oscillation between the two condensation states with opposite phases and different coupling: in-phase for y_{high} and antiphase for y_{low} . **e-g**, Diagrams of spin configurations of condensations y_{high} , x and y_{low} corresponding to the real-space images of **b**, **c** and **d**, respectively. Panels **e** and **f** show the antiferromagnetic coupling (solid blue lines) with parallel spins, and **g** shows ferromagnetic coupling (dashed blue lines) with antiparallel spins between neighbouring sites. Scale bars in **b**, **c** and **d**, $2 \mu\text{m}$.

substrates. Two of these DBR substrates were then bonded together via a thermal compression bonding process with prepatterned gold pillars as the spacers (Methods and Supplementary Fig. 3), creating a symmetric two-dimensional (2D) confined nanocavity (Fig. 1b) to serve as the optical cavity as well as the crystal growth environment. Chemical reaction and crystal growth under nanometre confinement are different than in traditional methods (Methods and Supplementary Fig. 1), and the resulting single-crystalline perovskite crystals are very large ($>300 \mu\text{m}$; Supplementary Fig. 4) due to a substantially decreased nucleation rate (Supplementary Fig. 6)²⁹. In addition, the nanoconfined environment also leads to evaporation only from the nanocavities' exposed edges, resulting in a slow crystal growth rate³⁰ and thus excellent crystallinity, as evidenced by the sharp X-ray diffraction peaks (Supplementary Fig. 5). To demonstrate its broad applicability, we synthesized three emerging excitonic halide perovskites (Supplementary Fig. 4)—the all-inorganic bromide perovskite CsPbBr_3 , the 2D iodide layered perovskite $(\text{C}_6\text{H}_5\text{C}_2\text{H}_4\text{NH}_3)_2\text{PbI}_4$ (phenylethylamine lead iodide, PEPI) and the organic-inorganic hybrid chloride perovskite MAPbCl_3 —all with submillimetre crystal sizes and high crystallinity (Supplementary Fig. 5). Compared with previously reported layer-by-layer stacking of polaritonic devices, our approach produced a laterally large size, yet vertically controllable, nanoscale-thin, single-crystalline halide perovskites free from damage or the contamination from traditional fabrication due to the use of prebonded ultra-flat DBR mirrors (Supplementary Figs. 7 and 8). At the same time, this fabrication design also produces pristine DBR optical reflectivity, which indicates excellent potential for future studies of near thermal equilibrium polariton BEC.

Our work combines large lateral size, nanometre-precision thickness control, homogeneity and excellent excitonic properties as required for large-scale room-temperature polaritonics. The precise control over the crystal thickness here enables accurate tuning of the photonic mode and hence the emission dynamics of the polariton mode. To demonstrate the excellent crystal thickness control and uniformity, we performed atomic force microscopy (AFM) of our

CsPbBr_3 crystal. The height profile (Fig. 1c) reveals a $329 \pm 0.4 \text{ nm}$ range ($\sim 0.12\%$ variance) across a lateral distance of $20 \mu\text{m}$ (Fig. 1c inset). This measured height matches well with the designed cavity height ($\sim 330 \text{ nm}$; Fig. 1b). By designing cavities of various heights (adjusting the pillar height between DBR substrates), we observed that the crystal grew to fill the cavities completely, with minimal deviation (Fig. 1d). The fully filled cavities in the perovskite chemical synthesis lead to excellent thickness homogeneity, which results in small polariton mode disorders (Supplementary Fig. 14); these cavities are distinct from the partially filled cavities in organics' physical recrystallization, which have substantial polariton mode inhomogeneity²⁷. Across 50 to 700 nm, the crystal thickness control shows nanometre-scale precision, with less than 1.6% of the variance across each chip (2 cm size) caused by pillar film deposition uniformity. In addition, we also achieved a cavity thickness down to $4.45 \pm 0.35 \text{ nm}$ (Fig. 1e and Supplementary Fig. 9), limiting the crystal thickness to a few unit cells. This quantum confinement even led to control over the excitonic energy level.

This method also allows us to fully take advantage of the perovskites' excellent optical properties. PL mapping under ultraviolet excitation showed excellent optical homogeneity (Fig. 1f and Supplementary Figs. 10 and 14); a long PL lifetime (Supplementary Fig. 11), pointing to low non-radiative loss; and a narrow PL emission peak (Supplementary Fig. 12). More importantly, robust excitons were observed at room temperature, supported by the strong excitonic absorption peak (Supplementary Fig. 13). The optical properties, combined with the high reflectivity of the DBR mirrors (cavity quality factor $Q \approx 900$ with two symmetric nine pairs DBR mirrors on both sides of the perovskites), resulted in the strongly coupled exciton polaritons (Fig. 1g). Due to the high optical quality and precise detuning control of the solution-grown CsPbBr_3 perovskite sample, a room-temperature polariton BEC at $k_{\parallel} = 0$ (k_{\parallel} is the in-xy-plane wavevector) with non-resonant excitation was readily observed (Supplementary Figs. 16 and 17).

More interestingly, due to the orthorhombic crystal structure of CsPbBr_3 at room temperature, optical birefringence breaks

the degeneracy of the two photonics transverse-electric and transverse-magnetic modes at $k_{\parallel}=0$ (ref. ²⁵; Fig. 1g). The combination of noticeable optical birefringence and spin-orbit coupling that arises from transverse-electric/transverse-magnetic mode splitting in CsPbBr₃ creates an interesting k-space dispersion³¹ (Fig. 1g) along with the x and y directions (two crystal axes as shown in Fig. 1f). This dispersion effectively creates a synthetic gauge field on the flowing polariton condensate and is predicted to be Rashba-like around the two diabolical points (Fig. 1g,h)³¹, where the two polariton branches exactly cross. In contrast to the organics^{32–34}, the nonlinearity and homogeneity in our perovskites are much superior. Thus, the perovskite microcavities also provide a unique room-temperature playground for future large-scale and nonlinear studies on non-Abelian gauge fields^{17,31,35} and topological physics³⁶.

Construction of XY spin Hamiltonian

Given the large and homogeneous samples with interesting polariton dispersion, we were able to explore the potential and limits of our approach by performing the room-temperature polariton graphs of the XY Hamiltonian minimizer demonstration with CsPbBr₃ perovskites. Many complex optimization problems can be mapped into microscopic spin models with rich macroscopic behaviours such as a distinct Kosterlitz-Thouless³⁷ phase transition. However, compared with other lithographically patterned polariton lattices^{38,39}, experimentally implementing XY Hamiltonian lattices at room temperature is one of the most challenging tasks due to the stringent sample requirements. Thus, a successful construction has only been reported at 10 K with the best MBE-grown GaAs quantum-well microcavities^{15,40}, where both excellent sample homogeneity (within a few millielectronvolts potential disorders/variations) and large sample size requirements can be met simultaneously.

Here, taking advantage of nanoconfinement-grown perovskites, we finally construct the polaritonic XY spin Hamiltonian at room temperature by non-resonantly exciting polariton lattice patterns with a reflective spatial light modulator (schematics in Supplementary Fig. 15). PL images of the condensate lattice were collected in a transmission configuration to control the excitation and the signal collection separately. Because of the strong polariton-polariton repulsive interaction originating from the Coulombic interaction among excitons, the polaritons under condensation will have a non-zero in-plane momentum and expand ballistically^{41,42} with a small excitation laser spot (Supplementary Fig. 18). When these expanding condensates are brought closer, interference and coupling occur, leading to phase synchronization between the condensates⁴³. According to the complex Ginzburg-Landau equation model in previous analysis¹⁵, the total amount of polaritons N_{XY} can be approximated as $N_{XY} = N_{iso} + \sum_{ij} J_{ij} \cos(\theta_i - \theta_j)$, where

N_{iso} is the total polariton number with full isolated sites (infinite distance), $\theta_i - \theta_j$ is the phase difference between two condensates and J_{ij} is the nearest neighbour coupling strength. The final macroscopic coherent state will have the highest possible polaritonic occupancy to minimize the polariton losses⁴⁴. Thus, in the ideal cases, the relative phase difference between condensates can be used as pseudo-spins and provides a route to search the global minimum in the XY Hamiltonian^{15,40,44}, $H_{XY} = -\sum_{ij} J_{ij} \cos(\theta_i - \theta_j)$. When the Josephson coupling is negligible, the coupling strength J_{ij} has an oscillating characteristic as a function of $k_c d$, where k_c is the outflow in-plane momentum and d is the distance between the two adjacent condensates.^{15,41} This results in ferromagnetic (positive sign) and antiferromagnetic (negative sign) couplings between sites, as demonstrated in Supplementary Figs. 22 and 23 for a polariton dyad configuration. Thus, by changing the geometry of the polariton lattice via a spatial light modulator, different XY spin Hamiltonians can be readily constructed.

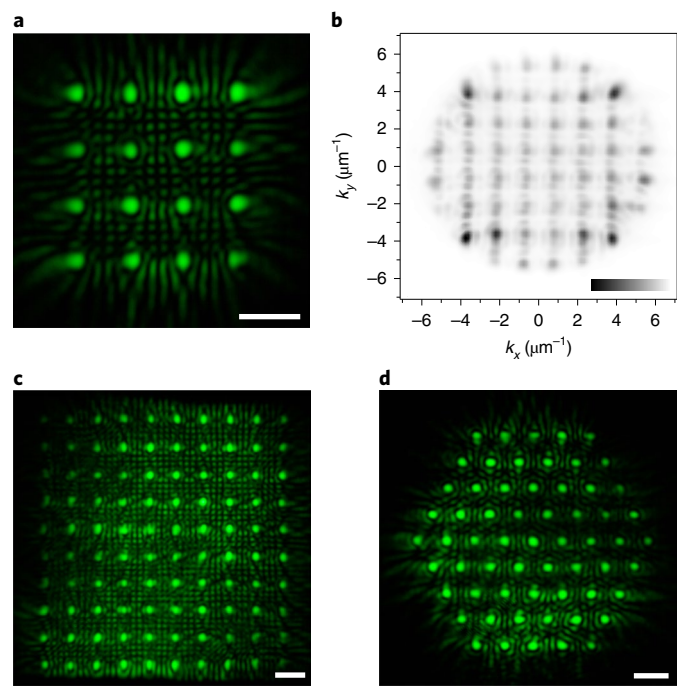


Fig. 3 | Extended polariton lattices. **a,b**, Time-integrated real-space and k-space images of a 4×4 polariton lattice with antiferromagnetic coupling. The even interference fringes can be clearly identified. In the colour bar in **b**, black is high intensity and white is low intensity. **c**, Time-integrated real-space image of a 10×10 polariton lattice with antiferromagnetic coupling. **d**, Time-integrated real-space image of a triangular polariton lattice with ferromagnetic coupling. Scale bars in **a**, **c** and **d**, 5 μm .

When a 2×2 lattice was excited in CsPbBr₃ microcavities with a fixed laser spot distance of $\sim 1.5 \mu\text{m}$, in contrast with GaAs, the two split lower polariton branches with perpendicular polarizations (Supplementary Fig. 18) condense simultaneously at three slightly different k-space locations (Fig. 2a). The x -polarization branch condenses at $k_c = 4.95 \mu\text{m}^{-1}$ with an odd number of interference fringes in k-space dispersion images (line of blue dots in Fig. 2a). The corresponding four real-space condensates (Fig. 2c) also have the same phase, indicating a ferromagnetic coupling as in the spin diagram shown in Fig. 2f. For the y -polarization branch, both ferromagnetic and antiferromagnetic configurations were identified. While the condensates with higher $k_c = 4.3 \mu\text{m}^{-1}$ (y_{high}) are synchronized to have the same phase (Fig. 2b), the lower $k_c = 3.2 \mu\text{m}^{-1}$ condensates (y_{low}) have a π phase difference between the neighbours (Fig. 2d). The antiphase interference effect also induces the condensates to be closer, consistent with low-temperature GaAs cases¹⁵. This coexistence of both in-phase and antiphase synchronization of the same polarization branch is due to the intrinsic oscillatory lattice dynamics⁴⁵. In addition, a 90° compass spin model can also be realized with an asymmetrical square configuration (Supplementary Fig. 25).

For the future study of phase transitions in interacting bosonic systems such as the Kosterlitz-Thouless transition with a polariton, it is essential to construct a large-scale, homogeneous and coherently coupled lattice. Towards this goal, we gradually increase the node number of the polariton lattices and tune the lattice geometry simply by dynamically changing the spatial light modulator excitation pattern. High-quality real-space and k-space images of a 4×4 polariton lattice (Fig. 3a,b) are first achieved. The even number of real-space interference fringes between the two neighbouring condensations (Fig. 3a) can be clearly seen, indicating an antiferromagnetic energy minimum state. In addition, the k-space image confirms the antiferromagnetic coupling with the characteristic

pattern, where the slightly lower-intensity centre spots are accompanied by higher-intensity Bragg diffraction peaks in the surrounding corner (Fig. 3b), similar to low-temperature GaAs cases¹⁵. Next, an 8×8 lattice is also easily constructed (Supplementary Fig. 26). In addition, the square lattice can be further extended to 10×10 coherently coupled condensates with a full lattice size of more than $50 \mu\text{m}$. Again, an even number of interference fringes with excellent visibility in between neighbouring condensates suggest an antiferromagnetic coupling. The inhomogeneity of the condensates at the edge region is mainly caused by the polariton outflow (the particle outflow to the sites on the edge happens from fewer sites in comparison with the central sites), as shown in Fig. 3 and Supplementary Fig. 24, instead of the small disorders in our samples (lower polariton-mode spatial root-mean-square variations of only 1.02 meV in Supplementary Fig. 14). These intensity inhomogeneities play an essential role in changing the interactions and the phase difference distribution⁴⁴, which can be addressed in the future with feedback excitation schemes recently reported⁴⁰. A real-space PL image of a sizable ($40 \mu\text{m}$) triangular lattice, one of the most important spin configurations in magnetism research^{2,15}, is also shown in Fig. 3d. In this case, the XY Hamiltonian is minimized when all polariton sites lock in phase and establish a ferromagnetic configuration.

Outlook

We emphasize that, to realize this room-temperature polaritonic XY Hamiltonian experiment, strongly interacting polaritons and large homogeneous samples are crucial to generate outflow condensates and to construct a large node lattice without being impacted by the crystal boundaries or disorders, respectively. Thanks to the Wannier–Mott excitons, the polariton–polariton interaction constant g (ref. ²³) in perovskite can be at least two orders of magnitude higher than in the organics with weakly interacting Frenkel excitons⁴⁶. The stringent requirements of homogeneity (one almost needs disorder free), photo-stability and large sample size further hinder other room-temperature systems^{10,11,24,25,47} from performing the above spin Hamiltonian experiments. In addition, the experimental room-temperature real-space polariton PL images from our solution-grown samples are comparable to the low-temperature MBE-grown GaAs case¹⁵, which further justifies the high quality of our perovskite platform. The interesting dispersions of perovskite can lead to three sets of XY Hamiltonian patterns, due to condensation at three different \mathbf{k} -space locations. Last but not least, future innovations on material platforms and optical technology are still highly sought to achieve practical XY spin Hamiltonian simulators for optimization problems, where one can precisely control the Hamiltonian at a more quantitative level with a substantially large lattice size.

To conclude, we solution-synthesized various types of halide perovskites using a nanoconfinement growth approach for room-temperature polaritonics. The resulting large-area but nanoscale-thickness crystals with excellent excitonic properties and homogeneity enabled us to demonstrate a polaritonic spin Hamiltonian lattice with a large size at room temperature. Our work establishes a robust room-temperature polaritonic platform for studying non-equilibrium physics. Given the pristine DBR optical reflectivity, the approach is also attractive for near thermal equilibrium polariton BEC at room temperature. The unique combination of intrinsically large optical birefringence and strongly nonlinear interacting polaritons is ideal for studies of quantum fluid physics in topological systems³¹ and simulating a lithography-patterned³⁹ large 2D Hamiltonian with spin-orbital coupling⁴⁸. The strong nonlinearity from Wannier–Mott excitons alone could also lead to many other device applications, such as a 2D topological polaritonic laser^{16,49} and potential photonic simulator with synthetic gauge field^{31,35}, previously inaccessible at room temperature.

Online content

Any methods, additional references, Nature Research reporting summaries, source data, extended data, supplementary information, acknowledgements, peer review information; details of author contributions and competing interests; and statements of data and code availability are available at <https://doi.org/10.1038/s41563-022-01276-4>.

Received: 22 July 2021; Accepted: 4 May 2022;

Published online: 9 June 2022

References

- Buluta, I. & Nori, F. Quantum simulators. *Science* **326**, 108–111 (2009).
- Struck, J. et al. Quantum simulation of frustrated classical magnetism in triangular optical lattices. *Science* **333**, 996–999 (2011).
- Gross, C. & Bloch, I. Quantum simulations with ultracold atoms in optical lattices. *Science* **357**, 995–1001 (2017).
- Deng, H., Haug, H. & Yamamoto, Y. Exciton-polariton Bose-Einstein condensation. *Rev. Mod. Phys.* **82**, 1489–1537 (2010).
- Boulter, T. et al. Microcavity polaritons for quantum simulation. *Adv. Quantum Technol.* **3**, 2000052 (2020).
- Byrnes, T., Kim, N. Y. & Yamamoto, Y. Exciton-polariton condensates. *Nat. Phys.* **10**, 803–813 (2014).
- Deng, H., Weihs, G., Santori, C., Bloch, J. & Yamamoto, Y. Condensation of semiconductor microcavity exciton polaritons. *Science* **298**, 199–202 (2002).
- Kasprzak, J. et al. Bose-Einstein condensation of exciton polaritons. *Nature* **443**, 409–414 (2006).
- Christopoulos, S. et al. Room-temperature polariton lasing in semiconductor microcavities. *Phys. Rev. Lett.* **98**, 126405 (2007).
- Plumhof, J. D., Stoeferle, T., Mai, L., Scherf, U. & Mahrt, R. Room-temperature Bose-Einstein condensation of cavity exciton-polaritons in a polymer. *Nat. Mater.* **13**, 247–252 (2014).
- Daskalakis, K. S., Maier, S. A., Murray, R. & Kéna-Cohen, S. Nonlinear interactions in an organic polariton condensate. *Nat. Mater.* **13**, 271–278 (2014).
- Kang, J. W. et al. Room temperature polariton lasing in quantum heterostructure nanocavities. *Sci. Adv.* **5**, eaau9338 (2019).
- Amo, A. et al. Polariton superfluids reveal quantum hydrodynamic solitons. *Science* **332**, 1167–1170 (2011).
- Sich, M. et al. Observation of bright polariton solitons in a semiconductor microcavity. *Nat. Photon.* **6**, 50–55 (2012).
- Berloff, N. G. et al. Realizing the classical XY Hamiltonian in polariton simulators. *Nat. Mater.* **16**, 1120–1126 (2017).
- Klembt, S. et al. Exciton-polariton topological insulator. *Nature* **562**, 552–556 (2018).
- Gianfrate, A. et al. Measurement of the quantum geometric tensor and of the anomalous Hall drift. *Nature* **578**, 381–385 (2020).
- Zhang, Q. et al. High-quality whispering-gallery-mode lasing from cesium lead halide perovskite nanoplatelets. *Adv. Funct. Mater.* **26**, 6238–6245 (2016).
- Passarelli, J. V. et al. Tunable exciton binding energy in 2D hybrid layered perovskites through donor–acceptor interactions within the organic layer. *Nat. Chem.* **12**, 672–682 (2020).
- Baranowski, M. & Plochocka, P. Excitons in metal-halide perovskites. *Adv. Energy Mater.* **10**, 1903659 (2020).
- Stranks, S. D. & Snaith, H. J. Metal-halide perovskites for photovoltaic and light-emitting devices. *Nat. Nanotechnol.* **10**, 391–402 (2015).
- Sutherland, B. R. & Sargent, E. H. Perovskite photonic sources. *Nat. Photon.* **10**, 295–302 (2016).
- Fieramosca, A. et al. Two-dimensional hybrid perovskites sustaining strong polariton interactions at room temperature. *Sci. Adv.* **5**, eaav967 (2019).
- Su, R. et al. Room-temperature polariton lasing in all-inorganic perovskite nanoplatelets. *Nano Lett.* **17**, 3982–3988 (2017).
- Bao, W. et al. Observation of Rydberg exciton polaritons and their condensate in a perovskite cavity. *Proc. Natl. Acad. Sci. USA* **116**, 20274–20279 (2019).
- Su, R. et al. Perovskite semiconductors for room-temperature exciton-polaritonics. *Nat. Mater.* **20**, 1315–1324 (2021).
- Kéna-Cohen, S., Davançó, M. & Forrest, S. R. Strong exciton-photon coupling in an organic single crystal microcavity. *Phys. Rev. Lett.* **101**, 116401 (2008).
- Wang, X. D., Li, W. G., Liao, J. F. & Kuang, D. B. Recent advances in halide perovskite single-crystal thin films: fabrication methods and optoelectronic applications. *Sol. RRL* **3**, 1800294 (2019).
- Chen, Z. et al. Thin single crystal perovskite solar cells to harvest below-bandgap light absorption. *Nat. Commun.* **8**, 1890 (2017).
- Liu, Y. et al. Multi-inch single-crystalline perovskite membrane for high-detectivity flexible photosensors. *Nat. Commun.* **9**, 5302 (2018).

31. Terças, H., Flayac, H., Solnyshkov, D. D. & Malpuech, G. Non-Abelian gauge fields in photonic cavities and photonic superfluids. *Phys. Rev. Lett.* **112**, 066402 (2014).
32. Kéna-Cohen, S., Davanço, M. & Forrest, S. R. Resonant Rayleigh scattering from an anisotropic organic single-crystal microcavity. *Phys. Rev. B* **78**, 153102 (2008).
33. Rechcinska, K. et al. Engineering spin-orbit synthetic Hamiltonians in liquid-crystal optical cavities. *Science* **366**, 727–730 (2019).
34. Ren, J. et al. Nontrivial band geometry in an optically active system. *Nat. Commun.* **12**, 689 (2021).
35. Whittaker, C. E. et al. Optical analogue of Dresselhaus spin-orbit interaction in photonic graphene. *Nat. Photon.* **15**, 193–196 (2021).
36. Su, R., Ghosh, S., Liew, T. C. H. & Xiong, Q. Optical switching of topological phase in a perovskite polariton lattice. *Sci. Adv.* **7**, eabf8049 (2021).
37. Kosterlitz, J. M. & Thouless, D. J. Ordering, metastability and phase transitions in two-dimensional systems. *J. Phys. C* **6**, 1181–1203 (1973).
38. Dusel, M. et al. Room temperature organic exciton–polariton condensate in a lattice. *Nat. Commun.* **11**, 2863 (2020).
39. Su, R. et al. Observation of exciton polariton condensation in a perovskite lattice at room temperature. *Nat. Phys.* **16**, 301–306 (2020).
40. Töpfer, J. D. et al. Engineering spatial coherence in lattices of polariton condensates. *Optica* **8**, 106–113 (2021).
41. Ohadi, H. et al. Nontrivial phase coupling in polariton multiplets. *Phys. Rev. X* **6**, 031032 (2016).
42. Wouters, M., Carusotto, I. & Ciuti, C. Spatial and spectral shape of inhomogeneous nonequilibrium exciton-polariton condensates. *Phys. Rev. B* **77**, 115340 (2008).
43. Tosi, G. et al. Geometrically locked vortex lattices in semiconductor quantum fluids. *Nat. Commun.* **3**, 1243 (2012).
44. Kalinin, K. P. & Berloff, N. G. Networks of non-equilibrium condensates for global optimization. *New J. Phys.* **20**, 113023 (2018).
45. Kalinin, K. P. & Berloff, N. G. Polaritonic network as a paradigm for dynamics of coupled oscillators. *Phys. Rev. B* **100**, 245306 (2019).
46. Lerario, G. et al. Room-temperature superfluidity in a polariton condensate. *Nat. Phys.* **13**, 837–841 (2017).
47. Luo, S. et al. Classical spin chains mimicked by room-temperature polariton condensates. *Phys. Rev. Appl.* **13**, 44052 (2020).
48. Whittaker, C. E. et al. Exciton polaritons in a two-dimensional Lieb lattice with spin-orbit coupling. *Phys. Rev. Lett.* **120**, 097401 (2018).
49. Liu, W. et al. Generation of helical topological exciton-polaritons. *Science* **370**, 600–604 (2020).

Publisher's note Springer Nature remains neutral with regard to jurisdictional claims in published maps and institutional affiliations.

© The Author(s), under exclusive licence to Springer Nature Limited 2022

Methods

Fabrication of optical cavity and nanocavity. For the fabrication of the DBR wafer, six inch quartz wafers were cleaned by soaking in heated 120 °C piranha baths for 10 min followed by a four-cycle deionized water wash. The cleaned wafers were loaded into a vacuum chamber for $\text{SiO}_2/\text{Ta}_2\text{O}_5$ deposition by electron beam evaporation with an advanced plasma source. Nine pairs of the $\text{SiO}_2/\text{Ta}_2\text{O}_5$ DBR mirror were deposited at 300 °C. The elevated temperature and high-kinetic-energy plasma bombardments produced sharp interfaces and improved each layer's film density, flatness and surface roughness and hence enhanced the optical quality of the DBR mirrors.

For the thermal compression of the wafer–wafer bonding of the DBR wafer with the patterned gold pillar, the DBR wafers were cleaned with piranha solution (same conditions as the cleaning of the quartz wafer, mentioned above). A 2D array of squared gold pads (side length, 250 μm ; thickness as designed; separation, 750 μm) were deposited on the surface of the DBR wafers by electron beam evaporation. Two of the same gold-patterned wafers were cleaned by deionized water for four cycles before being loaded into the wafer bonder. The wafers were aligned according to the position of the gold pads followed by slowly increasing the compressive force to 20,000 N. The chamber was slowly ramped up to 300 °C in 30 min and kept there for 100 min before naturally cooling overnight with the compressive force on. The bonded wafer was finally diced into small chips for crystal growth. One can also use copper or SiO_2 as the bonding spacer at the expense of a higher processing temperature.

Synthesis of halide perovskites. All of the chemicals were purchased from Sigma-Aldrich Chemical and used as received. Unless specified, all the solution preparation and crystal growth were carried out in an argon-filled glove box (though there was no noticeable quality difference compared with ambient condition synthesis).

For the growth of the all-inorganic halide perovskite (CsPbBr_3) thin crystals in the nanocavity, we used an inverse temperature crystallization. First, 1 ml dimethyl sulfoxide DMSO was added into a caesium bromide (CsBr , 1 mmol, 0.212 g) and lead bromide (PbBr_2 , 2 mmol, 0.734 g) powder mixture in a 10 ml vial. Violent vibration was used until all powder dissolved at room temperature before filtration to remove possible impurities. A drop of the prepared solution was dropped at the edge of the fabricated DBR nanocavity, and 10 min was given until the cavity space was fully filled by the solution through capillary force. The DBR nanocavity with CsPbBr_3 precursor solution was put on a hot plate, and the temperature was ramped up to 120 °C in 2 min and kept there for 24 hours. The perovskite growth locations were random in the cavity. After the crystal growth, the DBR nanocavity with crystals was put in a vacuum chamber to remove possible residual solvent.

For the growth of 2D halide perovskite (PEPI) thin crystals in the nanocavity, the method is an induced peripheral crystallization. First, 1 ml γ -butyrolactone was added into a phenylethylamine iodide (1 mmol, 0.249 g) and lead iodide (2 mmol, 0.922 g) powder mixture in a 10 ml vial. Violent vibration was used until all the powders were dissolved at room temperature before filtration to remove possible impurities. A drop of the prepared solution was dropped at the edge of the fabricated DBR nanocavity, and 10 min was given until the cavity space was fully filled with the solution through capillary force. The DBR nanocavity with PEPI precursor solution was put on a hot plate, the temperature was ramped up to 100 °C in 2 min and kept there overnight. The temperature was slowly cooled at a rate of 10 °C h^{-1} to room temperature to let the PEPI crystal grow. The perovskite growth locations were random in the cavity.

For the growth of the hybrid halide perovskite (methylammonium lead chloride) thin crystals in the nanocavity, we adopted an inversion temperature precision gradient crystallization. First, 1 ml mixed solvent (N,N -dimethylformamide and dimethyl sulfoxide, 1:1, v/v) was added into a methylammonium chloride (1 mmol, 0.067 g) and lead chloride (1 mmol, 0.278 g) powder mixture in a 10 ml vial. Violent vibration was used until all the powder was dissolved at room temperature before filtration to remove possible impurities. A drop of the prepared solution was dropped at the edge of the fabricated DBR nanocavity, and 10 min was given until the cavity space was fully filled with the solution through capillary force. The DBR nanocavity with methylammonium chloride precursor solution was put on a hot plate, and the temperature was ramped up to 80 °C in 2 min and maintained there for 4 h before ramping up to 100 °C and being kept there for 24 h. The perovskite growth locations were random in the cavity. After the crystal growth, the DBR nanocavity with crystals was put in a vacuum chamber to remove possible residual solvent.

For the CVD growth of all-inorganic CsPbBr_3 perovskite, the all-inorganic perovskites shown in the Supplementary Information were synthesized via a one-step approach using a single-zone CVD system. Freshly cleaved high-quality mica substrates (1.2 cm × 4 cm) were placed on top of a quartz crucible containing a powder mixture of CsBr (20 mg) and PbBr_2 (30 mg) before being sent into the centre of a CVD tube. The tube was pumped down and fed with Ar (99.999% purity) four times. Tube pressure was maintained at ambient pressure with an Ar flow rate of 30 sccm. The system was first heated to 400 °C within 24 min, followed by heating from 400 °C to 500 °C within 4 min and being maintained for 20 min. After the growth of crystals, the tube was cooled to room temperature naturally.

Characterizations of halide perovskites. For the AFM, the nanocavities were opened by brute force with tweezers to expose the perovskite crystals before AFM measurements. The AFM images and height profiles of crystals were taken with a Park Systems NX10 AFM instrument in tapping mode and analysed withXEI software. Only the standard plane flattening process was used in our AFM data processing, this is a basic plane levelling used to remove the sample tilting effect from the image acquisition process.

All optical microscopy images of the halide perovskite crystals were taken using an Olympus microscope. Fluorescence microscopy images of PEPI and CsPbBr_3 were taken using the same Olympus microscope. The fluorescence microscopy image of MAPbCl_3 was taken by a Zeiss confocal microscope under ultraviolet excitation.

X-ray diffraction pattern measurements were taken using a D8 Discover GADDS powder X-ray diffractometer with $\text{Cu K}\alpha$ (wavelength, $\lambda = 1.54056 \text{ \AA}$).

For the ultraviolet-visible absorption spectrum and steady-state PL measurements, all absorption spectrum measurements were taken using a home-built ultraviolet-visible transmission set-up, which utilizes a collimated white lamp source and an Andor spectrometer equipped with a 2D electron multiplying charge coupled device. The PL spectra were performed by the same system. A 250 fs optical parametric amplifier pulse laser with a repetition rate of 20 kHz was used to pump non-resonantly.

All scanning electron microscopy images were taken with a FEI Nova NanoSEM 650.

The PL lifetime was measured using a home-built multifunctional microscope integrated with a time-correlated single-photon counting system. A femtosecond pulsed laser centred at 808 nm (Coherent Mira 900-F) was used for second harmonic generation at 404 nm via a barium borate crystal, and the produced 404 nm laser was fibre coupled to the microscope and focused on the samples through an objective lens. The PL was collected by the same objective and fibre coupled to a single-photon counting module (Excelitas SPCM AQRH 13) after blocking the 404 nm excitation. The PL photon counts were then time correlated (IDQuantique ID 900) with the sync signal from the pulsed laser to build the histogram of photon arrival time, from which PL lifetime can be extracted. Nanocavities were opened by brute force with tweezers before lifetime measurements.

Optical measurements of polariton. The optical measurements were performed using a home-built transmission set-up at room temperature as shown in Supplementary Fig. 15. A 250 fs optical parametric amplifier pulse laser with a repetition rate of 20 kHz was used to achieve non-resonant excitation (470 nm centre wavelength). A Meadowlark Optics reflective liquid-crystal phase-only spatial light modulator was used to generate excitation laser patterns. The hologram was computed with a Gerchberg-Saxton algorithm and transferred to an objective (Nikon $\times 40$ Plan Fluor ELWD, numerical aperture = 0.6) with a Fourier imaging configuration to generate a desired laser pattern on the focal plane. The PL was collected in a transmission configuration. The diameter of each focused laser spot was around 1.5 μm . From the other side of the microcavity, another objective was used to collect the PL. The k-space images can be obtained by a Fourier imaging configuration with two achromatic tube lenses. An Andor spectrometer equipped with a 2D electron multiplying charge coupled device was used to measure the energy-resolved polariton dispersions. A charge coupled device camera was used to obtain 2D k-space images and real-space images by flipping the first achromatic tube lens. A long-pass filter was used to filter the excitation laser.

The linear-polarized PL dispersions can be measured with a halfwave plate and a linear polarizer (as shown in Supplementary Fig. 15). A rotation stage was used to rotate the sample to obtain the dispersions along the x and y axes in Fig. 1g. The cross-section of the two polariton branches in k-space at the diabolic points in Fig. 1h was measured with two narrow-band Semrock bandwidth filters.

Reporting summary. Further information on research design is available in the Nature Research Reporting Summary linked to this article.

Data availability

The authors declare that the main data supporting the findings of this study are available within the paper. Extra data are available from the corresponding authors upon reasonable request. Source data are provided with this paper.

Acknowledgements

We thank P. James Schuck and F. Xue for reading the manuscript and valuable comments and A. Gao from SVOTEK Inc. for assisting with the high-quality DBR mirror coating. W.B. and K.P. acknowledge support from the Office of Naval Research (award no. N00014-21-1-2099) and National Science Foundation (award no. OIA-2044049). W.B. thanks the CAREER support from the National Science Foundation (award no. DMR-2143041). X.Z. and R.T. thank the support by the Gordon and Betty Moore Foundation (award no. 5722) and the Ernest S. Kuh Endowed Chair Professorship. S.K.-C. and L.H. acknowledge funding from the Canada Research Chairs programme and the Army Research Office (W911NF1810149). The work of Q.L. and G.R.F. was supported by the US Department of Energy, Office of Science, Basic Energy Science, Chemical

Sciences, Geosciences, and Biosciences Division. Use of the Center for Nanoscale Materials, a US Department of Energy Office of Science User Facility, was supported by the US Department of Energy, Office of Basic Energy Sciences under contract no. DE-AC02-06CH11357.

Author contributions

W.B., X.Z., R.T. and K.P. initiated the project and conceived the experiments. R.T. fabricated the microcavities and grew and characterized the perovskite materials. K.P. performed all optical measurements except lifetime characterizations. Q.L. and G.R.F. performed the PL lifetime experiments. S.K.-C., D.J. and L.H. provided valuable insight and suggestions. W.B. and X.Z. supervised the whole project. R.T., K.P. and W.B. prepared the initial draught of the manuscript. K.P., W.B., R.T. and X.Z. led the efforts in revising the manuscript with the other authors' participation.

Competing interests

The authors declare no competing interests.

Additional information

Supplementary information The online version contains supplementary material available at <https://doi.org/10.1038/s41563-022-01276-4>.

Correspondence and requests for materials should be addressed to Xiang Zhang or Wei Bao.

Peer review information *Nature Materials* thanks Natalia Berloff, Hui Deng and the other, anonymous, reviewer(s) for their contribution to the peer review of this work.

Reprints and permissions information is available at www.nature.com/reprints.

Corresponding author(s): Xiang Zhang

Last updated by author(s): May 3, 2022

Reporting Summary

Nature Portfolio wishes to improve the reproducibility of the work that we publish. This form provides structure for consistency and transparency in reporting. For further information on Nature Portfolio policies, see our [Editorial Policies](#) and the [Editorial Policy Checklist](#).

Statistics

For all statistical analyses, confirm that the following items are present in the figure legend, table legend, main text, or Methods section.

n/a Confirmed

- The exact sample size (n) for each experimental group/condition, given as a discrete number and unit of measurement
- A statement on whether measurements were taken from distinct samples or whether the same sample was measured repeatedly
- The statistical test(s) used AND whether they are one- or two-sided
Only common tests should be described solely by name; describe more complex techniques in the Methods section.
- A description of all covariates tested
- A description of any assumptions or corrections, such as tests of normality and adjustment for multiple comparisons
- A full description of the statistical parameters including central tendency (e.g. means) or other basic estimates (e.g. regression coefficient) AND variation (e.g. standard deviation) or associated estimates of uncertainty (e.g. confidence intervals)
- For null hypothesis testing, the test statistic (e.g. F , t , r) with confidence intervals, effect sizes, degrees of freedom and P value noted
Give P values as exact values whenever suitable.
- For Bayesian analysis, information on the choice of priors and Markov chain Monte Carlo settings
- For hierarchical and complex designs, identification of the appropriate level for tests and full reporting of outcomes
- Estimates of effect sizes (e.g. Cohen's d , Pearson's r), indicating how they were calculated

Our web collection on [statistics for biologists](#) contains articles on many of the points above.

Software and code

Policy information about [availability of computer code](#)

Data collection

Provide a description of all commercial, open source and custom code used to collect the data in this study, specifying the version used OR state that no software was used.

Data analysis

Provide a description of all commercial, open source and custom code used to analyse the data in this study, specifying the version used OR state that no software was used.

For manuscripts utilizing custom algorithms or software that are central to the research but not yet described in published literature, software must be made available to editors and reviewers. We strongly encourage code deposition in a community repository (e.g. GitHub). See the Nature Portfolio [guidelines for submitting code & software](#) for further information.

Data

Policy information about [availability of data](#)

All manuscripts must include a [data availability statement](#). This statement should provide the following information, where applicable:

- Accession codes, unique identifiers, or web links for publicly available datasets
- A description of any restrictions on data availability
- For clinical datasets or third party data, please ensure that the statement adheres to our [policy](#)

The authors declare that the main data supporting the findings of this study are available within the paper. Extra data are available from the corresponding authors upon reasonable request. Source data are provided with this paper.

Field-specific reporting

Please select the one below that is the best fit for your research. If you are not sure, read the appropriate sections before making your selection.

Life sciences Behavioural & social sciences Ecological, evolutionary & environmental sciences

For a reference copy of the document with all sections, see nature.com/documents/nr-reporting-summary-flat.pdf

Life sciences study design

All studies must disclose on these points even when the disclosure is negative.

Sample size	Describe how sample size was determined, detailing any statistical methods used to predetermine sample size OR if no sample-size calculation was performed, describe how sample sizes were chosen and provide a rationale for why these sample sizes are sufficient.
Data exclusions	Describe any data exclusions. If no data were excluded from the analyses, state so OR if data were excluded, describe the exclusions and the rationale behind them, indicating whether exclusion criteria were pre-established.
Replication	Describe the measures taken to verify the reproducibility of the experimental findings. If all attempts at replication were successful, confirm this OR if there are any findings that were not replicated or cannot be reproduced, note this and describe why.
Randomization	Describe how samples/organisms/participants were allocated into experimental groups. If allocation was not random, describe how covariates were controlled OR if this is not relevant to your study, explain why.
Blinding	Describe whether the investigators were blinded to group allocation during data collection and/or analysis. If blinding was not possible, describe why OR explain why blinding was not relevant to your study.

Behavioural & social sciences study design

All studies must disclose on these points even when the disclosure is negative.

Study description	Briefly describe the study type including whether data are quantitative, qualitative, or mixed-methods (e.g. qualitative cross-sectional, quantitative experimental, mixed-methods case study).
Research sample	State the research sample (e.g. Harvard university undergraduates, villagers in rural India) and provide relevant demographic information (e.g. age, sex) and indicate whether the sample is representative. Provide a rationale for the study sample chosen. For studies involving existing datasets, please describe the dataset and source.
Sampling strategy	Describe the sampling procedure (e.g. random, snowball, stratified, convenience). Describe the statistical methods that were used to predetermine sample size OR if no sample-size calculation was performed, describe how sample sizes were chosen and provide a rationale for why these sample sizes are sufficient. For qualitative data, please indicate whether data saturation was considered, and what criteria were used to decide that no further sampling was needed.
Data collection	Provide details about the data collection procedure, including the instruments or devices used to record the data (e.g. pen and paper, computer, eye tracker, video or audio equipment) whether anyone was present besides the participant(s) and the researcher, and whether the researcher was blind to experimental condition and/or the study hypothesis during data collection.
Timing	Indicate the start and stop dates of data collection. If there is a gap between collection periods, state the dates for each sample cohort.
Data exclusions	If no data were excluded from the analyses, state so OR if data were excluded, provide the exact number of exclusions and the rationale behind them, indicating whether exclusion criteria were pre-established.
Non-participation	State how many participants dropped out/declined participation and the reason(s) given OR provide response rate OR state that no participants dropped out/declined participation.
Randomization	If participants were not allocated into experimental groups, state so OR describe how participants were allocated to groups, and if allocation was not random, describe how covariates were controlled.

Ecological, evolutionary & environmental sciences study design

All studies must disclose on these points even when the disclosure is negative.

Study description	Briefly describe the study. For quantitative data include treatment factors and interactions, design structure (e.g. factorial, nested, hierarchical), nature and number of experimental units and replicates.
Research sample	Describe the research sample (e.g. a group of tagged <i>Passer domesticus</i> , all <i>Stenocereus thurberi</i> within Organ Pipe Cactus National

Research sample

Monument), and provide a rationale for the sample choice. When relevant, describe the organism taxa, source, sex, age range and any manipulations. State what population the sample is meant to represent when applicable. For studies involving existing datasets, describe the data and its source.

Sampling strategy

Note the sampling procedure. Describe the statistical methods that were used to predetermine sample size OR if no sample-size calculation was performed, describe how sample sizes were chosen and provide a rationale for why these sample sizes are sufficient.

Data collection

Describe the data collection procedure, including who recorded the data and how.

Timing and spatial scale

Indicate the start and stop dates of data collection, noting the frequency and periodicity of sampling and providing a rationale for these choices. If there is a gap between collection periods, state the dates for each sample cohort. Specify the spatial scale from which the data are taken

Data exclusions

If no data were excluded from the analyses, state so OR if data were excluded, describe the exclusions and the rationale behind them, indicating whether exclusion criteria were pre-established.

Reproducibility

Describe the measures taken to verify the reproducibility of experimental findings. For each experiment, note whether any attempts to repeat the experiment failed OR state that all attempts to repeat the experiment were successful.

Randomization

Describe how samples/organisms/participants were allocated into groups. If allocation was not random, describe how covariates were controlled. If this is not relevant to your study, explain why.

Blinding

Describe the extent of blinding used during data acquisition and analysis. If blinding was not possible, describe why OR explain why blinding was not relevant to your study.

Did the study involve field work? Yes No

Field work, collection and transport

Field conditions

Describe the study conditions for field work, providing relevant parameters (e.g. temperature, rainfall).

Location

State the location of the sampling or experiment, providing relevant parameters (e.g. latitude and longitude, elevation, water depth).

Access & import/export

Describe the efforts you have made to access habitats and to collect and import/export your samples in a responsible manner and in compliance with local, national and international laws, noting any permits that were obtained (give the name of the issuing authority, the date of issue, and any identifying information).

Disturbance

Describe any disturbance caused by the study and how it was minimized.

Reporting for specific materials, systems and methods

We require information from authors about some types of materials, experimental systems and methods used in many studies. Here, indicate whether each material, system or method listed is relevant to your study. If you are not sure if a list item applies to your research, read the appropriate section before selecting a response.

Materials & experimental systems

- | | |
|--------------------------|--|
| n/a | Involved in the study |
| <input type="checkbox"/> | <input type="checkbox"/> Antibodies |
| <input type="checkbox"/> | <input type="checkbox"/> Eukaryotic cell lines |
| <input type="checkbox"/> | <input type="checkbox"/> Palaeontology and archaeology |
| <input type="checkbox"/> | <input type="checkbox"/> Animals and other organisms |
| <input type="checkbox"/> | <input type="checkbox"/> Human research participants |
| <input type="checkbox"/> | <input type="checkbox"/> Clinical data |
| <input type="checkbox"/> | <input type="checkbox"/> Dual use research of concern |

Methods

- | | |
|--------------------------|---|
| n/a | Involved in the study |
| <input type="checkbox"/> | <input type="checkbox"/> ChIP-seq |
| <input type="checkbox"/> | <input type="checkbox"/> Flow cytometry |
| <input type="checkbox"/> | <input type="checkbox"/> MRI-based neuroimaging |

Antibodies

Antibodies used

Describe all antibodies used in the study; as applicable, provide supplier name, catalog number, clone name, and lot number.

Validation

Describe the validation of each primary antibody for the species and application, noting any validation statements on the manufacturer's website, relevant citations, antibody profiles in online databases, or data provided in the manuscript.

Eukaryotic cell lines

Policy information about [cell lines](#)

Cell line source(s)

State the source of each cell line used.

Authentication

Describe the authentication procedures for each cell line used OR declare that none of the cell lines used were authenticated.

Mycoplasma contamination

Confirm that all cell lines tested negative for mycoplasma contamination OR describe the results of the testing for mycoplasma contamination OR declare that the cell lines were not tested for mycoplasma contamination.

**Commonly misidentified lines
(See [ICLAC](#) register)**

Name any commonly misidentified cell lines used in the study and provide a rationale for their use.

Palaeontology and Archaeology

Specimen provenance

Provide provenance information for specimens and describe permits that were obtained for the work (including the name of the issuing authority, the date of issue, and any identifying information). Permits should encompass collection and, where applicable, export.

Specimen deposition

Indicate where the specimens have been deposited to permit free access by other researchers.

Dating methods

If new dates are provided, describe how they were obtained (e.g. collection, storage, sample pretreatment and measurement), where they were obtained (i.e. lab name), the calibration program and the protocol for quality assurance OR state that no new dates are provided.

Tick this box to confirm that the raw and calibrated dates are available in the paper or in Supplementary Information.

Ethics oversight

Identify the organization(s) that approved or provided guidance on the study protocol, OR state that no ethical approval or guidance was required and explain why not.

Note that full information on the approval of the study protocol must also be provided in the manuscript.

Animals and other organisms

Policy information about [studies involving animals](#); [ARRIVE guidelines](#) recommended for reporting animal research

Laboratory animals

For laboratory animals, report species, strain, sex and age OR state that the study did not involve laboratory animals.

Wild animals

Provide details on animals observed in or captured in the field; report species, sex and age where possible. Describe how animals were caught and transported and what happened to captive animals after the study (if killed, explain why and describe method; if released, say where and when) OR state that the study did not involve wild animals.

Field-collected samples

For laboratory work with field-collected samples, describe all relevant parameters such as housing, maintenance, temperature, photoperiod and end-of-experiment protocol OR state that the study did not involve samples collected from the field.

Ethics oversight

Identify the organization(s) that approved or provided guidance on the study protocol, OR state that no ethical approval or guidance was required and explain why not.

Note that full information on the approval of the study protocol must also be provided in the manuscript.

Human research participants

Policy information about [studies involving human research participants](#)

Population characteristics

Describe the covariate-relevant population characteristics of the human research participants (e.g. age, gender, genotypic information, past and current diagnosis and treatment categories). If you filled out the behavioural & social sciences study design questions and have nothing to add here, write "See above."

Recruitment

Describe how participants were recruited. Outline any potential self-selection bias or other biases that may be present and how these are likely to impact results.

Ethics oversight

Identify the organization(s) that approved the study protocol.

Note that full information on the approval of the study protocol must also be provided in the manuscript.

Clinical data

Policy information about [clinical studies](#)

All manuscripts should comply with the ICMJE [guidelines for publication of clinical research](#) and a completed [CONSORT checklist](#) must be included with all submissions.

Clinical trial registration

Provide the trial registration number from ClinicalTrials.gov or an equivalent agency.

Study protocol

Note where the full trial protocol can be accessed OR if not available, explain why.

Data collection

Describe the settings and locales of data collection, noting the time periods of recruitment and data collection.

Outcomes

Describe how you pre-defined primary and secondary outcome measures and how you assessed these measures.

Dual use research of concern

Policy information about [dual use research of concern](#)

Hazards

Could the accidental, deliberate or reckless misuse of agents or technologies generated in the work, or the application of information presented in the manuscript, pose a threat to:

No	Yes
<input type="checkbox"/>	<input type="checkbox"/> Public health
<input type="checkbox"/>	<input type="checkbox"/> National security
<input type="checkbox"/>	<input type="checkbox"/> Crops and/or livestock
<input type="checkbox"/>	<input type="checkbox"/> Ecosystems
<input type="checkbox"/>	<input type="checkbox"/> Any other significant area

Experiments of concern

Does the work involve any of these experiments of concern:

No	Yes
<input type="checkbox"/>	<input type="checkbox"/> Demonstrate how to render a vaccine ineffective
<input type="checkbox"/>	<input type="checkbox"/> Confer resistance to therapeutically useful antibiotics or antiviral agents
<input type="checkbox"/>	<input type="checkbox"/> Enhance the virulence of a pathogen or render a nonpathogen virulent
<input type="checkbox"/>	<input type="checkbox"/> Increase transmissibility of a pathogen
<input type="checkbox"/>	<input type="checkbox"/> Alter the host range of a pathogen
<input type="checkbox"/>	<input type="checkbox"/> Enable evasion of diagnostic/detection modalities
<input type="checkbox"/>	<input type="checkbox"/> Enable the weaponization of a biological agent or toxin
<input type="checkbox"/>	<input type="checkbox"/> Any other potentially harmful combination of experiments and agents

ChIP-seq

Data deposition

- Confirm that both raw and final processed data have been deposited in a public database such as [GEO](#).
- Confirm that you have deposited or provided access to graph files (e.g. BED files) for the called peaks.

Data access links

May remain private before publication.

For "Initial submission" or "Revised version" documents, provide reviewer access links. For your "Final submission" document, provide a link to the deposited data.

Files in database submission

Provide a list of all files available in the database submission.

Genome browser session (e.g. [UCSC](#))

Provide a link to an anonymized genome browser session for "Initial submission" and "Revised version" documents only, to enable peer review. Write "no longer applicable" for "Final submission" documents.

Methodology

Replicates

Describe the experimental replicates, specifying number, type and replicate agreement.

Sequencing depth

Describe the sequencing depth for each experiment, providing the total number of reads, uniquely mapped reads, length of reads and whether they were paired- or single-end.

Antibodies

Describe the antibodies used for the ChIP-seq experiments; as applicable, provide supplier name, catalog number, clone name, and lot number.

Peak calling parameters

Specify the command line program and parameters used for read mapping and peak calling, including the ChIP, control and index files used.

Data quality

Describe the methods used to ensure data quality in full detail, including how many peaks are at FDR 5% and above 5-fold enrichment.

Software

Describe the software used to collect and analyze the ChIP-seq data. For custom code that has been deposited into a community repository, provide accession details.

Flow Cytometry

Plots

Confirm that:

- The axis labels state the marker and fluorochrome used (e.g. CD4-FITC).
- The axis scales are clearly visible. Include numbers along axes only for bottom left plot of group (a 'group' is an analysis of identical markers).
- All plots are contour plots with outliers or pseudocolor plots.
- A numerical value for number of cells or percentage (with statistics) is provided.

Methodology

Sample preparation

Describe the sample preparation, detailing the biological source of the cells and any tissue processing steps used.

Instrument

Identify the instrument used for data collection, specifying make and model number.

Software

Describe the software used to collect and analyze the flow cytometry data. For custom code that has been deposited into a community repository, provide accession details.

Cell population abundance

Describe the abundance of the relevant cell populations within post-sort fractions, providing details on the purity of the samples and how it was determined.

Gating strategy

Describe the gating strategy used for all relevant experiments, specifying the preliminary FSC/SSC gates of the starting cell population, indicating where boundaries between "positive" and "negative" staining cell populations are defined.

- Tick this box to confirm that a figure exemplifying the gating strategy is provided in the Supplementary Information.

Magnetic resonance imaging

Experimental design

Design type

Indicate task or resting state; event-related or block design.

Design specifications

Specify the number of blocks, trials or experimental units per session and/or subject, and specify the length of each trial or block (if trials are blocked) and interval between trials.

Behavioral performance measures

State number and/or type of variables recorded (e.g. correct button press, response time) and what statistics were used to establish that the subjects were performing the task as expected (e.g. mean, range, and/or standard deviation across subjects).

Acquisition

Imaging type(s)

Specify: functional, structural, diffusion, perfusion.

Field strength

Specify in Tesla

Sequence & imaging parameters

Specify the pulse sequence type (gradient echo, spin echo, etc.), imaging type (EPI, spiral, etc.), field of view, matrix size, slice thickness, orientation and TE/TR/flip angle.

Area of acquisition

State whether a whole brain scan was used OR define the area of acquisition, describing how the region was determined.

Diffusion MRI

Used

Not used

Preprocessing

Preprocessing software

Provide detail on software version and revision number and on specific parameters (model/functions, brain extraction, segmentation, smoothing kernel size, etc.).

Normalization

If data were normalized/standardized, describe the approach(es): specify linear or non-linear and define image types used for transformation OR indicate that data were not normalized and explain rationale for lack of normalization.

Normalization template

Describe the template used for normalization/transformation, specifying subject space or group standardized space (e.g. original Talairach, MNI1305, ICBM152) OR indicate that the data were not normalized.

Noise and artifact removal

Describe your procedure(s) for artifact and structured noise removal, specifying motion parameters, tissue signals and physiological signals (heart rate, respiration).

Volume censoring

Define your software and/or method and criteria for volume censoring, and state the extent of such censoring.

Statistical modeling & inference

Model type and settings

Specify type (mass univariate, multivariate, RSA, predictive, etc.) and describe essential details of the model at the first and second levels (e.g. fixed, random or mixed effects; drift or auto-correlation).

Effect(s) tested

Define precise effect in terms of the task or stimulus conditions instead of psychological concepts and indicate whether ANOVA or factorial designs were used.

Specify type of analysis: Whole brain ROI-based Both

Statistic type for inference
(See [Eklund et al. 2016](#))

Specify voxel-wise or cluster-wise and report all relevant parameters for cluster-wise methods.

Correction

Describe the type of correction and how it is obtained for multiple comparisons (e.g. FWE, FDR, permutation or Monte Carlo).

Models & analysis

n/a Involved in the study

- Functional and/or effective connectivity
- Graph analysis
- Multivariate modeling or predictive analysis

Functional and/or effective connectivity

Report the measures of dependence used and the model details (e.g. Pearson correlation, partial correlation, mutual information).

Graph analysis

Report the dependent variable and connectivity measure, specifying weighted graph or binarized graph, subject- or group-level, and the global and/or node summaries used (e.g. clustering coefficient, efficiency, etc.).

Multivariate modeling and predictive analysis

Specify independent variables, features extraction and dimension reduction, model, training and evaluation metrics.